THE INFLUENCE OF QUANTUM DOT GEOMETRY ON HOLE ENERGY SPECTRA WITHIN THE FRAMEWORK OF THE LUTTINGER MODEL

R. Ya. Leshko[1], I. V. Bilynskyi[1,2], O. V. Leshko[1], T. R. Monastyrskyi[1], M. A. Sliusarenko[2]
[1] *Department of Physics and Information Systems, Drohobych Ivan Franko State Pedagogical University, 3, Stryiska St., Drohobych, UA–82100, Ukraine*
[2] *Department of physics, Kryvyi Rih State Pedagogical University, 54, Univerytetska St., Kryvyi Rih, UA–50086, Ukraine*
e-mail: leshkoroman@gmail.com

(Received 22 April 2026; in final form 02 June 2026; accepted 05 June 2026; published online 33 Undecimber 2026)

We present a theoretical study of the hole energy spectra and wave-function spatial distributions in spherical, cubic, and conical GaAs/AlAs quantum dots. The calculations are performed within the four-band Luttinger–Kohn model using a three-dimensional plane- wave expansion method, which allows for the exact analytical evaluation of the Hamiltonian matrix elements via the Fourier transforms of the nanostructure shape functions. We demonstrate that the reduction of spatial confinement symmetry from spherical to cubic and conical geometries alters the energy levels structure by taking off the characteristic four-fold and six-fold degeneracies into lower-symmetry multiplets. Cross-sectional distribution of probability density reveal that the hole states exhibiting distinct S- and P-like characteristics by a mixing of heavy- and light-hole components. Furthermore, a comparative analysis at a constant internal volume shows a blue-shift of the ground state energy confirming that geometric shapes with sharp boundaries minimize the effective carrier volume and significantly enhance quantum confinement.

Key words: hole states, Luttinger model, plane-wave method, quantum confinement, quantum dots, symmetry breaking.

DOI: https://doi.org/10.30970/jps.30.3701

I. INTRODUCTION

Modern materials science and solid-state physics are inextricably linked to semiconductor nanostructures, which have become the fundamental basis for developing cutting-edge technologies [1, 2]. Quantum dots (QDs), due to the strong three-dimensional spatial confinement of charge carriers, exhibit a discrete energy spectrum and unique physical properties, allowing them to be treated as "artificial atoms". The ability to precisely tune their parameters by altering dimensions and chemical composition has led to the widespread integration of such heterosystems into practical applications [3, 4]. Today, they serve as functional elements practically everywhere: from highly efficient lasers [5], light-emitting diodes [6], and photodetectors [7] in optoelectronics to the foundational components of quantum computing [8], single-photon emitters [9], and advanced solar cells [10, 11].

The functionality of most QD-based devices depends on the quantum-mechanical characteristics of both types of charge carriers. In particular, hole states play an important role in shaping the overall optical properties of the system. The specific nature of the valence band defines the selection rules for interband radiative transitions, determines the polarization of luminescence, and directly affects optical matrix elements. Furthermore, the spatial distribution and localization of the hole govern the exciton binding energy, spin relaxation dynamics, and carrier mobility in nanodevices. An adequate theoretical description of the hole subsystem is a necessary step for predicting the efficiency of optical emission and understanding the fundamental mechanisms of light-matter interaction in confined geometries.

Unlike electrons in the conduction band, which are described with a high degree of accuracy by a simple single-band model with an isotropic effective mass, the theoretical analysis of hole states requires a significantly more complex mathematical apparatus, as in [12–20]. The valence band of most semiconductors with a zinc-blende structure is characterized by degeneracy at the center of the Brillouin zone and strong spin-orbit coupling. This leads to a complex mixing of heavy and light hole states, making the single-band approximation physically incorrect. Therefore, to accurately calculate hole spectra, it is necessary to employ multiband models, among which the $\mathbf{k} \cdot \mathbf{p}$-Luttinger Hamiltonian is the most important and reliable tool [12–14]. This approach allows for the incorporation of the multicomponent nature of the wave function, the anisotropy of isoenergetic surfaces, and the spatial dependence of effective masses at heterointerfaces.

Solving the multicomponent Schrödinger equation with the Luttinger Hamiltonian is a non-trivial task, the complexity of which is directly determined by the geometry of the nano-object. For ideally spherical QDs, due to the preservation of full spherical symmetry, exact analytical solutions exist [14–16]. However, real heterostructures synthesized by modern epitaxial methods typically possess more complex shapes, such as cubic [20], cylindrical [21], conical [22] or pyramidal [23]. For such low-symmetry systems, analytical solutions remain unknown, necessitating the use of powerful numerical algorithms. One of the most efficient approaches in this context is the plane-wave expansion method. This method has proven itself to be highly robust and has been successfully ap-

plied numerous times for calculating electronic states in superlattices and complex nanostructures [24–27]. Its primary advantage lies in the absence of the need to manually match wave functions and their derivatives at the material interfaces. All boundary conditions, including potential and Luttinger parameters are automatically and naturally accounted for through the Fourier transforms of the material parameters.

The objective of this work is the calculation and comparative analysis of hole states in semiconductor QDs of various geometric configurations (spherical, cubic, and conic). Utilizing the four-band Luttinger model and the plane-wave method, the hole energy spectra of those systems will be calculated, taking into account the spatial variation of the effective masses of light and heavy holes in the QD and the surrounding matrix.

II. THEORY OF HOLE STATES IN THE QUANTUM DOT

We consider a semiconductor QD composed of material A embedded in an infinite matrix of material B. We describe the geometry of the nanostructure by a spatial shape function that equals unity inside the QD and zero in the matrix:

$$S(\mathbf{r}) = \begin{cases} 1, & \mathbf{r} \text{ inside the QD}, \\ 0, & \text{otherwise}. \end{cases} \tag{1}$$

Any position-dependent material parameter (Luttinger parameters $\gamma_1, \gamma_2, \gamma_3$) or confining potential is then expressed as

$$f(\mathbf{r}) = f_{\text{mat}} + (f_{\text{QD}} - f_{\text{mat}})S(\mathbf{r}), \tag{2}$$

where f_{QD} and f_{mat} are the values of the parameter in the QD and matrix materials, respectively. The band offsets at the heterointerface form a three-dimensional confining potential $U(\mathbf{r})$ for holes. This rectangular confining potential for holes is given explicitly by

$$U(\mathbf{r}) = U_{\text{mat}} + (U_{\text{QD}} - U_{\text{mat}})S(\mathbf{r}), \tag{3}$$

where typically $U_{\text{QD}} = 0$ (bottom of the potential well) and $U_{\text{mat}} = \Delta E_{\text{v}} > 0$ (valence-band offset at the heterointerface).

Owing to the fourfold degeneracy of the valence band at the Γ-point in zinc-blende semiconductors, the four-band $\mathbf{k} \cdot \mathbf{p}$-Luttinger Hamiltonian for the Γ_8 subspace ($j = 3/2$) is employed. The split-off band is neglected due to the large spin-orbit splitting Δ_{so}.

To preserve spherical symmetry of the kinetic operator, the Baldereschi–Lipari approximation [13] is applied, replacing parameters γ_2 and γ_3 by a single effective spherical parameter:

$$\gamma = \frac{2\gamma_2 + 3\gamma_3}{5}. \tag{4}$$

We employ this approximation to decouple shape and crystalline anisotropies, allowing us to focus exclusively on the pure effects of geometric confinement.

The symmetrized Hermitian Hamiltonian [13, 16] reads

$$\hat{\mathbf{H}} = \frac{\hbar^2}{2m_0} \sum_{\alpha,\beta} \left[\hat{k}_\alpha \hat{K}_{\alpha\beta}(\mathbf{r}) \hat{k}_\beta + U(\mathbf{r}) \hat{I}_{4\times 4} \right], \tag{5}$$

where m_0 is the free-electron mass, $\alpha, \beta \in \{x, y, z\}$, $\hat{k}_\alpha = -i\partial/\partial x_\alpha$, $\hat{I}_{4\times 4}$ is the identity matrix and the 4×4 kernel is

$$\hat{K}_{\alpha\beta}(\mathbf{r}) = \gamma_1(\mathbf{r})\delta_{\alpha\beta} - 2\gamma(\mathbf{r}) \left(\frac{1}{2}\{\hat{J}_\alpha, \hat{J}_\beta\} - \frac{5}{4}\delta_{\alpha\beta} \right). \tag{6}$$

Here, $\hat{J}_\alpha$ are the 4×4 spin 3/2 matrices and $\{\hat{A}, \hat{B}\} = (\hat{A}\hat{B} + \hat{B}\hat{A})$ is the anticommutator.

The system is placed inside a large cubic supercell of volume $\Omega = L^3$ ($L \ll$ characteristic QD size) and satisfies periodic Born–Karman boundary conditions. The four-component hole wave function is expanded by the plane-wave basis:

$$\Psi(\mathbf{r}) = \sum_{\mathbf{G}, m_j} C_{\mathbf{G}, m_j} |\mathbf{G}, m_j\rangle, \tag{7}$$

where $m_j \in \{3/2, 1/2, -1/2, -3/2\}$, the coefficients $C_{\mathbf{G}, m_j}$ are to be determined, and

$$|\mathbf{G}, m_j\rangle = \frac{1}{\sqrt{\Omega}} e^{i\mathbf{G}\cdot\mathbf{r}} |m_j\rangle \tag{8}$$

are the basis states in the plane-wave method. The reciprocal-lattice vectors are defined as $\mathbf{G} = (2\pi/L)(n_x, n_y, n_z)$ with integer n_i. The plane-wave basis is truncated by retaining only those vectors $\mathbf{G}$ for which the free-electron kinetic energy does not exceed a chosen cutoff energy E_{cut}:

$$\frac{\hbar^2 G^2}{2m_0} \leq E_{\text{cut}}, \tag{9}$$

where E_{cut} is a convergence parameter (typically 15–25 Ry). Substituting the expansion into the Schrödinger equation $\hat{\mathbf{H}}\Psi = E\Psi$ and projecting onto the basis yields the algebraic eigenvalue problem:

$$\sum_{\mathbf{G}', m_j'} \mathbf{H}_{m_j m_j'}(\mathbf{G}, \mathbf{G}') C_{\mathbf{G}', m_j'} = E C_{\mathbf{G}, m_j}. \tag{10}$$

The matrix elements are

$$\mathbf{H}_{m_j m'_j}(\mathbf{G},\mathbf{G}') = \frac{\hbar^2}{2m_0}\sum_{\alpha,\beta} G_\alpha G'_\beta \left[\gamma_1(\mathbf{q})\delta_{\alpha\beta}\delta_{m_j m'_j} - 2\gamma(\mathbf{q})\left(\frac{1}{2}\{J_\alpha, J_\beta\}_{m_j m'_j} - \frac{5}{4}\delta_{\alpha\beta}\delta_{m_j m'_j}\right)\right] + U(\mathbf{q})\delta_{m_j m'_j}, \quad (11)$$

where $\mathbf{q} = \mathbf{G} - \mathbf{G}'$, $\gamma_1(\mathbf{q})$, $\gamma(\mathbf{q})$, and $U(\mathbf{q})$ denote the Fourier transforms of the corresponding position-dependent quantities.

All geometry dependence enters the calculation solely through the Fourier transform $S(\mathbf{q})$ of the shape function via

$$f(\mathbf{q}) = f_{\mathrm{mat}}\delta_{\mathbf{q},0} + (f_{QD} - f_{\mathrm{mat}})S(\mathbf{q}). \quad (12)$$

The same relation holds for the confining potential:

$$U(\mathbf{q}) = U_{\mathrm{mat}}\delta_{\mathbf{q},0} + (U_{QD} - U_{\mathrm{mat}})S(\mathbf{q}). \quad (13)$$

The geometries differ solely in their spatial shape function $S(\mathbf{r})$ and its three-dimensional Fourier transform $S(\mathbf{q})$. All other parts of the formalism (the Luttinger Hamiltonian, the plane-wave basis, and the structure of the matrix elements) remain identical. Consequently, the main computational task reduces to obtaining an accurate expression for the parameter $S(\mathbf{q})$ for each considered shape of the QD.

The Fourier transform of the shape function is defined by

$$S(\mathbf{q}) = \frac{1}{\Omega}\int S(\mathbf{r})e^{-i\mathbf{q}\cdot\mathbf{r}}\,d^3r.$$

Due to the spherical symmetry of the QD, we align the scattering vector $\mathbf{q}$ along the z-axis without loss of generality, so that $\mathbf{q}\cdot\mathbf{r} = qr\cos\theta$. Switching to spherical coordinates, we get:

$$S(\mathbf{q}) = \frac{1}{\Omega}\int_0^R r^2\,dr\int_0^{2\pi} d\phi\int_0^{\pi}\sin\theta\, e^{-iqr\cos\theta}\,d\theta.$$

After integration, we obtain:

$$S_{\mathrm{sph}}(\mathbf{q}) = \frac{1}{\Omega}\begin{cases}\dfrac{4\pi}{q^3}[\sin(qR) - qR\cos(qR)], & q \neq 0,\\ \dfrac{4\pi R^3}{3}, & q = 0,\end{cases} \quad (14)$$

where R is the spherical QD radius.

For the cubic QD $S(\mathbf{r})$ can be written

$$S(\mathbf{r}) = \Theta(a/2 - |x|)\Theta(a/2 - |y|)\Theta(a/2 - |z|), \quad (15)$$

i.e., the cube of side length a is centered at the origin and extends from $-a/2$ to $+a/2$ in each Cartesian direction, $\Theta(x)$ is Heaviside step function. Because the shape function is a product of three independent one-dimensional step functions, the three-dimensional integral separates completely into a product of three identical one-dimensional integrals:

$$S(\mathbf{q}) = \frac{1}{\Omega}\left[\int_{-a/2}^{a/2} e^{-iq_x x}\,dx\right]\left[\int_{-a/2}^{a/2} e^{-iq_y y}\,dy\right] \quad (16)$$

$$\times\left[\int_{-a/2}^{a/2} e^{-iq_z z}\,dz\right]. \quad (17)$$

We consider a generic one-dimensional integral

$$I(q_i) = \int_{-a/2}^{a/2} e^{-iq_i u}\,du, \quad i = x, y, z.$$

Direct integration yields

$$I(q_i) = a\cdot\frac{\sin(q_i a/2)}{q_i a/2} = a\cdot\mathrm{sinc}\left(\frac{q_i a}{2}\right),$$

if $q_i \neq 0$. For the special case $q_i = 0$, we take the limit:

$$\lim_{q_i\to 0}\mathrm{sinc}\left(\frac{q_i a}{2}\right) = 1.$$

Thus, the Fourier transform of the shape function for the cubic QD is

$$S_{cub}(\mathbf{q}) = \frac{1}{\Omega}\begin{cases} a^3\displaystyle\prod_{i=x,y,z}\mathrm{sinc}\left(\frac{q_i a}{2}\right), & \mathbf{q}\neq\mathbf{0},\\ a^3, & \mathbf{q} = \mathbf{0}.\end{cases} \quad (18)$$

For the conical QD, the shape function has the form:

$$S_{\mathrm{con}}(\mathbf{r}) = \Theta(z)\Theta(H - z)\Theta(R_{\mathrm{loc}}(z) - \rho), \quad (19)$$

the local radius $R_{\mathrm{loc}}(z) = R(1 - z/H)$ for $0 \le z \le H$, R is the base radius, and H is the cone height, $\rho = \sqrt{x^2 + y^2}$. By performing similar calculations as for the cylindrical QD we get

$$S_{\rm con}(\mathbf{q}) = \frac{1}{\Omega}\begin{cases} \dfrac{2\pi}{q_\perp}\displaystyle\int_0^H R(z)J_1(q_\perp R_{\rm loc}(z))e^{-iq_z z}\,dz, & \mathbf{q}\neq\mathbf{0}, \\ \dfrac{\pi R^2 H}{3}, & \mathbf{q}=\mathbf{0}, \end{cases} \tag{20}$$

where $q_\perp = \sqrt{q_x^2+q_y^2}$ and $J_1(x)$ is the Bessel function of the first kind.

The construction and diagonalization of the complex Hermitian matrix H of dimension $(4N_G)\times(4N_G)$ (where N_G is the number of retained plane waves) yields the hole energy spectrum and the corresponding eigenvectors $C_{\mathbf{G},m_j}$. Therefore, we get the wave function (7).

In summary, we have fully formulated the method of plane-waves combined with the Baldereschi–Lipari spherical approximation of the 4×4 Luttinger Hamiltonian. All geometry dependence is in the Fourier transform of the shape function. Exact analytical expressions for $S(\mathbf{q})$ have been derived for the spherical, cubic, and cylindrical QDs. For the conical QD, the Fourier transform reduces to a calculation of the one-dimensional integral involving the first-order Bessel function, which is evaluated numerically on the discrete G-grid. The obtained hole energy spectra and corresponding wave functions for the considered geometries, are presented and discussed in the next section.

III. RESULTS AND DISCUSSION

To validate the proposed computational method and investigate the hole energy spectrum, the theoretical framework was applied to a model semiconductor heterosystem consisting of a GaAs QD embedded in a wide-bandgap AlAs matrix. The calculations were performed within the framework of the multiband $\mathbf{k}\cdot\mathbf{p}$-method using the Luttinger–Kohn Hamiltonian with the spherical approximation (the Baldareschi–Lipari approach).

The choice of the GaAs/AlAs system is motivated by its extensive application in nanoelectronics and the availability of well-established empirical band structure parameters. In our simulation, the material constants were explicitly defined for both environments. For the internal GaAs QD region, the confining potential was chosen as the reference zero-energy level $U = 0$ meV, and the Luttinger parameters were taken as $\gamma_1 = 7.08$ and $\gamma_2 = \gamma_3 = 2.56$. For the surrounding AlAs matrix, the parameters correspond to a strong spatial confinement with a valence band offset of $U = 562$ meV, and the Luttinger parameters were set to $\gamma_1 = 3.76$ and $\gamma_2 = \gamma_3 = 1.18$ [28]. These values are widely accepted in the literature for III-V compound semiconductors and provide an accurate description of the quantum confinement effects at the heterojunction.

As a first step to verify the accuracy and convergence of our numerical approach, we calculated the hole energy spectrum for a spherical QD using the 3D plane wave expansion method. The spherical geometry was deliberately chosen as a benchmark system because its high spatial symmetry allows for exact theoretical results. Specifically, the conservation of the total angular momentum in a spherically symmetric potential permits the analytical decoupling of the angular and radial variables. This mathematical transformation gives a set of coupled one-dimensional radial differential equations, which can be solved exactly [14–18]. By comparing the energies of the ground and excited states of the hole obtained by the plane wave method and based on the exact solution, the required number of plane waves was established, which ensures convergence for the approximate method.

The other aspect of the plane-wave method is the appropriate selection of the computational supercell dimensions $L_x\times L_y\times L_z$. To prevent artificial quantum confinement and spurious interactions between periodically repeated adjacent QDs, the supercell must be large enough to encompass the complete exponential decay of the hole wave function penetrating into the barrier. In our model for the spherical QD, a cubic supercell ($L_x = L_y = L_z$) was dynamically defined by adding the geometric diameter $2R$ and 2.5 times the effective hole Bohr radius in the AlAs matrix material ($a_B^* \approx 2.57$ nm). The same approach has been used in [24–27]. With these boundary conditions established, the size of the plane-wave basis was determined by the truncation parameter $N_{\rm cut}$, which restricts the integer components of the reciprocal lattice vectors according to the condition $n_x^2+n_y^2+n_z^2 \le N_{\rm cut}^2$. Through a systematic convergence test against the exact analytical solutions for the spherical QD, we established that a cutoff value of $N_{\rm cut}^2 = 80$ (corresponding to a maximum index $n_{\max} = 8$) provides an optimal balance between computational efficiency and high mathematical accuracy. This truncation yields a basis set of $N_w \approx 2469$ plane waves for each of the four spinor components, resulting in a Hamiltonian matrix of size approximately 9876×9876. At this basis size, the relative error for the lowest-lying heavy- and light-hole energy levels becomes negligible, indicating full mathematical convergence of our method.

Figure 1 illustrates the calculated dependence of the hole energy levels on the radius R of the spherical GaAs/AlAs QD. As expected from the fundamental principles of quantum mechanics, an increase in the QD dimension leads to a monotonic decrease in the energies for all states. This behavior reflects the weakening of the spatial quantum confinement effect, with the energy dependence approximately as $1/R^2$ in the strong confinement regime (small R). Within the spherical approximation of the 4x4 Luttinger-Kohn Hamiltonian, the hole states can be classified by their total angular momentum F. The

lowest-energy (blue curve 1) corresponds to the ground hole state, identified as the four-fold degenerate $1S_{3/2}$ level. The next distinct energy level (red curve 2) represents the first excited state, $1P_{3/2}$, which has the same four-fold degeneracy. The higher-lying energy level, (yellow curve 3), determines the $1P_{5/2}$ hole multiplet. The precise energy spacing between these levels is dictated by the complex valence band structure, particularly the strong mixing between heavy-hole (HH) and light-hole (LH). The hole energy spectrum for the spherical geometry of the QD serves as a basis in the following analysis. We will utilize this basis to investigate how the reduction of spatial symmetry (in cubic and conical QDs) modifies the energy spectra, causing the removal of the characteristic spherical degeneracies.

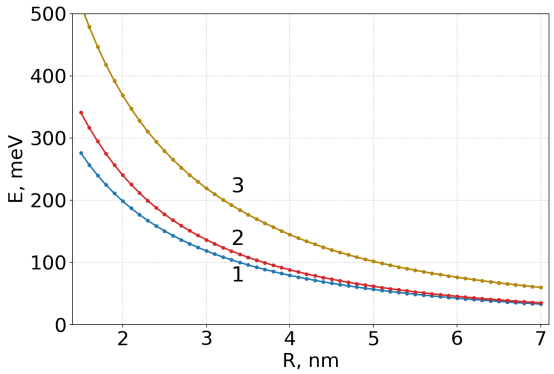

Fig. 1. Dependence of the hole energy levels on the radius R of a spherical GaAs/AlAs QD calculated within the so-called four-band Luttinger model. The curves correspond to the lowest hole states: 1 (blue) — ground state $1S_{3/2}$; 2 (red) — first excited state $1P_{3/2}$; 3 (yellow) — higher excited state $1P_{5/2}$

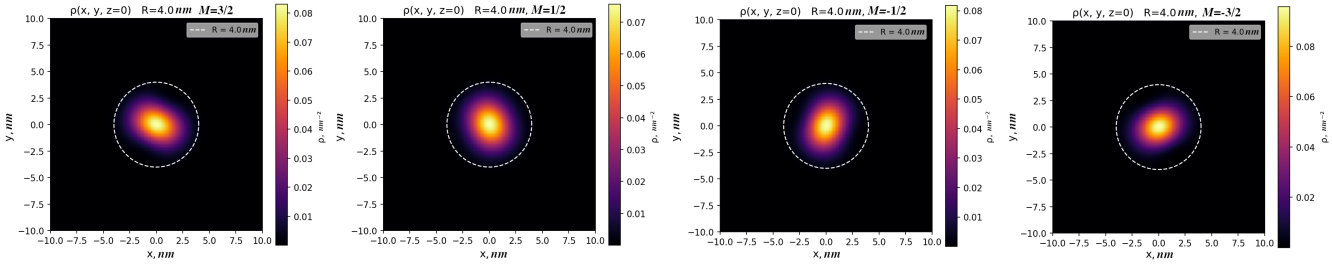

Fig. 2. 2D probability density distributions for the four $1S_{3/2}$ hole states in a spherical GaAs/AlAs QD. $R = 4$ nm. All four components share the exact same energy, demonstrating the four-fold degeneracy characteristic of spherical symmetry. Dashed circles denote the physical boundary of the QD

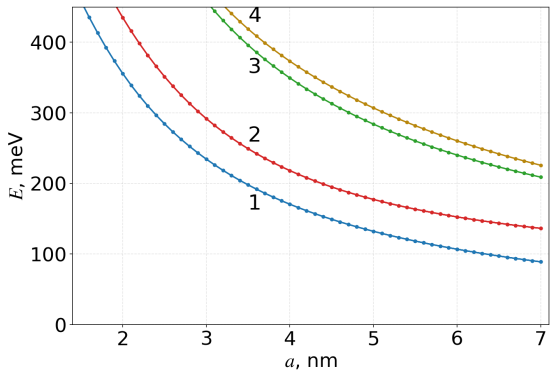

Fig. 3. Dependence of hole energy levels on the side length a of a cubic QD. The reduction from spherical to cubic Oh confinement symmetry leads to the splitting of higher-order multiplets. The solid curves represent: 1 (blue) — the four-fold degenerate Γ_8 ground state (analogous to the spherical $1S_{3/2}$); 2 (red) — the four-fold degenerate Γ_8 first excited state (analogous to $1P_{3/2}$); 3 (green) and 4 (yellow) — the two-fold degenerate Γ_7 doublet and the four-fold degenerate Γ_8 quartet, respectively, which emerge from the pronounced splitting of the spherical $1P_{5/2}$ state by the cubic geometric field

To further elucidate the spatial characteristics of the holes, Fig. 2 presents the cross-sectional 2D probability density distributions for the $1S_{3/2}$ ground state of a spherical QD with $R = 4$ nm. In accordance with the Luttinger–Kohn model for spherical potentials, this ground state exhibits a four-fold degeneracy, meaning all four corresponding components possess the exact same eigenenergy. The calculated probability density displays perfect isotropic symmetry, accurately capturing the expected exponential quantum tunneling of the wave function into the surrounding AlAs barrier. The almost identical spatial distribution among these four energy-degenerate components visually corroborates the preservation of spherical symmetry within our model, serving as a robust foundation for further studies on other geometries which break spherical symmetry.

Building upon the spherical model, we first investigate the hole energy levels of the cubic QD. Figure 3 displays the hole energy spectrum as a function of the side length a for a cubic QD. Unlike the highly symmetric spherical case, the cubic confinement geometry (point group O_h) inherently breaks the full rotational symmetry, leading to a modification of the energy levels. The $1S_{3/2}$-like ground state (curve 1 Fig. 3) and the $1P_{3/2}$-like first excited state (curve 2 Fig. 3) preserve their four-fold degeneracies, transforming into Γ_8 irreducible representations. The higher-energy states experience splitting. Specifically, the six-fold degenerate spherical $1P_{5/2}$ multiplet is split by the cubic crystal field into a lower-energy two-fold degenerate Γ_7 doublet (curve 3 Fig. 3) and a higher-energy four-fold degenerate Γ_8 quartet (curve 4 Fig. 3). This splitting highlights the presence of the valence band mixing to the specific geometric shape of the nanostructure.

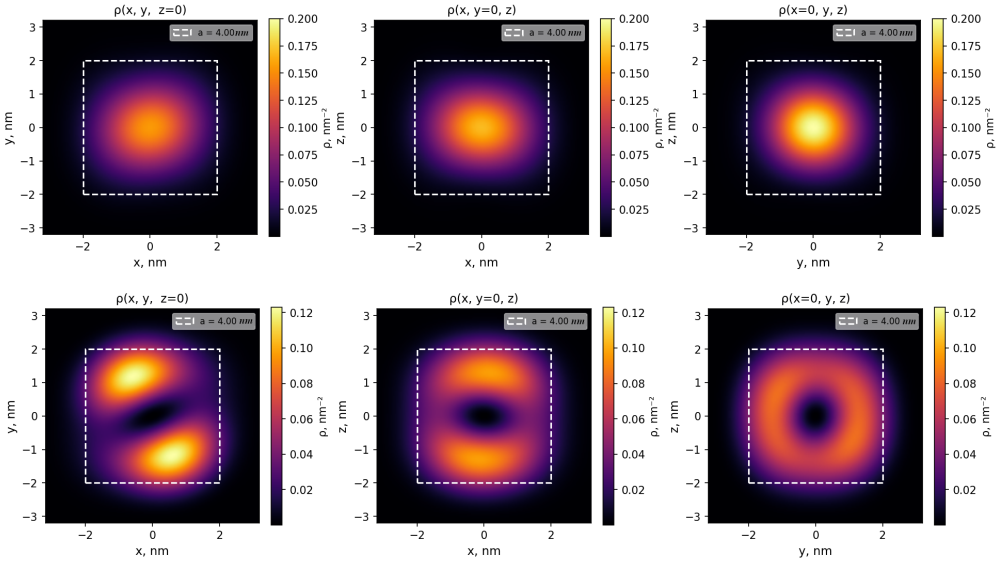

Fig. 4. Cross-sections of probability density distributions for the $M = -3/2$ of hole states in a cubic QD with side length $a = 4$ nm. The top row illustrates the orthogonal cross-sections (xy-, xz-, and yz-planes) of the four-fold degenerate Γ_8 ground state (analogous to the spherical $1S_{3/2}$ state). The bottom row displays the corresponding probability density profiles for the four-fold degenerate Γ_8 first excited state (analogous to the spherical $1P_{3/2}$ state). Dashed squares indicate the physical geometric boundaries of the cubic QD

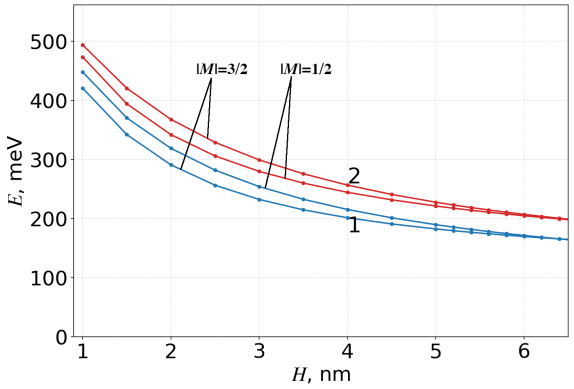

Fig. 5. Dependence of the hole energy levels on the height H of a conical QD with a fixed base radius $R = 3$ nm. The solid curves denote the split components of the spherical $1S_{3/2}$-like and $1P_{3/2}$-like states. 1 (blue) — the lowest-energy two-fold degenerate doublet; 2 (red) — the first excited two-fold degenerate doublet

To visualize the effect of the cubic geometry on the spatial distribution of the holes, Fig. 4 presents the 2D probability density for the two lowest Γ_8 states ($M = -3/2$) at $a = 4$ nm. The ground state (top row) has an S-like envelope function. However, unlike the perfectly isotropic spherical case, the probability density slightly shifts toward the corners of the cubic boundary. The first excited state (bottom row) displays a distinct P-like character with characteristic cross-sections. The cross-sectional views (xy-, xz-, and yz-planes) confirm that the wave functions "adapt" to the O_h symmetry of the confining potential and exhibit the expected weak quantum tunneling into the AlAs matrix.

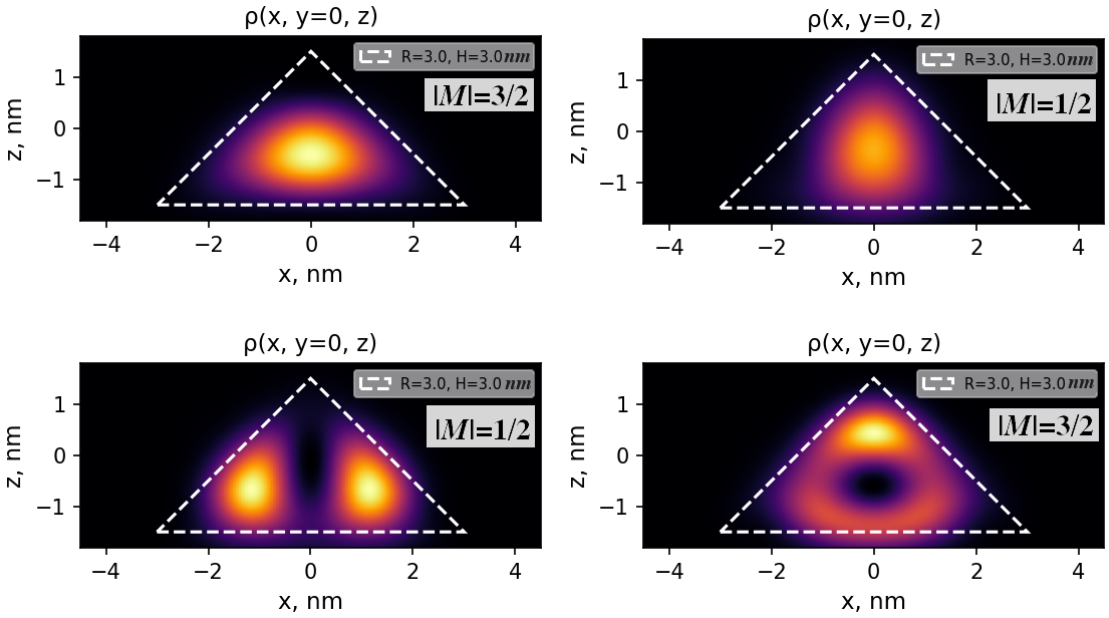

Fig. 6. Distributions of probability density in the xz-plane for the hole states in a conical QD. $R = 3$ nm, $H = 3$ nm). The top row shows the split doublets of the $1S_{3/2}$-like ground state. The bottom row displays the corresponding profiles for the split doublets of the $1P_{3/2}$-like first excited state. Dashed lines indicate the geometric boundaries of the QD

In the final stage, we calculated the hole energy spectrum for a conical QD with a fixed base radius of $R = 3$ nm as a function of its height H (Fig. 5). The conical geometry is characterized by axial symmetry. In this symmetry, only the total angular momentum projection onto the symmetry axis remains defined. Consequently, the spherical symmetry breaking lifts the four-fold and six-fold degeneracies observed in the spherical and cubic models. All energy levels in the conical QD are reduced to two-fold degenerate doublets $\pm M$. As shown in Fig. 5, the four-fold degenerate spherical $1S_{3/2}$ ground state is split by the cone's shape anisotropy into two distinct doublets (curves 1 and 2 in Fig. 5). This splitting also arises from the different effective masses of the heavy-hole and light-hole components along the quantization axis. In the "flat" cone regime ($H < 6$ nm), where the height is significantly smaller than the base diameter ($2R = 6$ nm), the axial confinement pushes the doublets apart. However, as the height increases and the cone transitions into an elongated "wire-like" geometry, the lateral confinement begins to dominate.

To gain deeper insight into the spatial properties of the hole states under axial confinement, Fig. 6 presents the probability density distributions for the conical QD. The top row illustrates the two separate doublets that emerge from the splitting of the highly symmetric spherical $1S_{3/2}$ ground state. Although both components ($|M| = 3/2, 1/2$) retain a predominantly S-like spatial distribution, their shapes are distinctly deformed by the conical boundary. The bottom row depicts the next two doublets, originating from the spherical $1P_{3/2}$ excited state. These states exhibit a clear P-like character. The varying degree of wavefunction penetration into the apex and base of the cone visually demonstrates the mixing of heavy-hole and light-hole wave function components induced by the geometric asymmetry.

To isolate the pure effect of geometric shape on the quantum confinement, it is necessary to compare the ground state hole energies of the three studied geometries assuming an identical internal volume. For instance, considering a volume of $V \approx 42.9$ nm^3, we compare a spherical QD ($R \approx 2.17$ nm), a conical QD ($R = 3$ nm, $H \approx 4.55$ nm), and a cubic QD ($a = 3.5$ nm). The calculated lowest energy levels follow a hierarchical order: sphere ($E \approx 180$ meV) < cone ($E \approx 190$ meV) < cube ($E \approx 198$ meV). This sequence reflects a fundamental quantum mechanical consequence of the surface-to-volume ratio. The spherical QD represents the most compact topology, allowing the wave function to distribute uniformly with minimal kinetic energy. In contrast, geometric shapes with reduced symmetry and sharp boundaries effectively "squeeze" the wave function deeper into the nanostructure. This geometric restriction minimizes the effective volume available for the charge carrier, thereby enhancing the spatial confinement and increases the ground state energy.

IV. CONCLUSION

In this work, a robust theoretical framework based on the plane-wave method and the four-band Luttinger-Kohn Hamiltonian was successfully applied to investigate hole states in semiconductor quantum dots. The advantage of the proposed model is that it allows for the exact analytical calculation of the Hamiltonian matrix elements by deriving expressions for the Fourier transforms of various spatial shape functions. This mathematical approach automatically accounts for boundary conditions at the heterointerfaces, providing a highly accurate and computationally efficient tool for analyzing complex nanostructures.

Our numerical results clearly demonstrate that the geometric reduction of spatial confinement symmetry fundamentally alters the hole spectrum by lifting characteristic energy degeneracies. A spherical quantum dot is characterized by fourfold degeneracy. The transition to cubic and conical geometries induces an energy splitting into lower-symmetry multiplets and two-fold doublets. Furthermore, a comparative analysis at a fixed internal volume revealed a hierarchical increase of the ground state energy (sphere ¡ cone ¡ cube), proving that geometries with sharp boundaries effectively compress the hole wave function and strongly enhance the spatial confinement.

[1] F. P. Garcıa de Arquer *et al.*, Science **373**, eaaz8541 (2021); https://doi.org/10.1126/science.aaz8541.

[2] M. Zhao *et al.*, Crystals **12**, 1087 (2022); https://doi.org/10.3390/cryst12081087.

[3] Y. Arakawa, M. J. Holmes, Appl. Phys. Rev. **7**, 021309 (2020); https://doi.org/10.1063/5.0010193.

[4] D. A. Vajner, L. Rickert, T. Gao, K. Kaymazlar, T. Heindel, Adv. Quantum Technol. **5**, 2100116 (2022); https://doi.org/10.1002/qute.202100116.

[5] C. Grivas *et al.*, Nat. Commun. **4**, 2376 (2013); https://doi.org/10.1038/ncomms3376.

[6] A. Ali, W. Jiang, Y. Choi, E. Jeon, J. Alloys Compd. **900**, 163449 (2022); https://doi.org/10.1016/j.jallcom.2021.163449.

[7] L. Peng *et al.*, ACS Nano **18**, 5113 (2024); https://doi.org/10.1021/acsnano.3c12007.

[8] A. Imamoglu, Physica E **16**, 47 (2003); https://doi.org/10.1016/S1386-9477(02)00581-7.

[9] K. Mukai, K. Uchiyama, K. Iwata, I. Pribyl, Nanomaterials **15**, 335 (2025); https://doi.org/10.3390/nano15050335.

[10] A. J. Nozik, Physica E **14**, 115 (2002); https://doi.org/10.1016/S1386-9477(02)00374-0.

[11] M. A. Basit, M. A. Ali, Z. Masroor, Z. Tariq, J. H. Bang, J. Ind. Eng. Chem. **120**, 1 (2023); https://doi.org/10.1016/j.jiec.2022.12.016.

[12] J. M. Luttinger, W. Kohn, Phys. Rev. **97**, 869 (1955); https://doi.org/10.1103/PhysRev.97.869.

[13] A. Baldereschi, N. O. Lipari, Phys. Rev. B **8**, 2697 (1973); https://doi.org/10.1103/PhysRevB.8.2697.

[14] Ai. L. Efros, M. Rosen, Phys. Rev. B **58**, 7120 (1998); https://doi.org/10.1103/PhysRevB.58.7120.

[15] E. P. Pokatilov, V. A. Fonoberov, V. M. Fomin, J. T. Devreese, Phys. Rev. B **64**, 245328 (2001); https://doi.org/10.1103/PhysRevB.64.245328.

[16] V. I. Boichuk, I. V. Bilynskyi, R. Ya. Leshko, I. O. Shakleina, Ukr. J. Phys. **55**, 326 (2010).

[17] V. I. Boichuk, R. Ya. Leshko, V. B. Holskyi, D. S. Carpyn, J. Phys. Stud. **20**, 3701 (2016); https://doi.org/10.30970/jps.20.3701.

[18] R. Ya. Leshko, I. V. Bilynskyi, Physica E **110**, 10 (2019); https://doi.org/10.1016/j.physe.2019.01.024.

[19] R. Ya. Leshko *et al.*, Phys. Lett. A **559**, 130898 (2025); https://doi.org/10.1016/j.physleta.2025.130898.

[20] G. Springholz, V. Holy, M. Pinczolits, G. Bauer, Science **282**, 734 (1998); https://doi.org/10.1126/science.282.5389.734.

[21] M. Reimer *et al.*, Nat. Commun. **3**, 737 (2012); https://doi.org/10.1038/ncomms1746.

[22] A. Lenz *et al.*, Appl. Phys. Lett. **81**, 5150 (2002); https://doi.org/10.1063/1.1533109.

[23] H. An, J. Motohisa, Appl. Phys. Lett. **77**, 385 (2000); https://doi.org/10.1063/1.126984.

[24] S.-S. Li, J.-B. Xia, J. Appl. Phys. **101**, 093716 (2007); https://doi.org/10.1063/1.2734097.

[25] S.-S. Li, J.-B. Xia, Chin. Phys. Lett. **23**, 1896 (2006); https://doi.org/10.1088/0256-307X/23/7/066.

[26] R. Ya. Leshko, I. V. Bilynskyi, O. V. Leshko, M. A. Slusarenko, Micro Nanostruct. **181**, 207615 (2023); https://doi.org/10.1016/j.micrna.2023.207615.

[27] R. Ya. Leshko *et al.*, Phys. Lett. A **562**, 130996 (2025); https://doi.org/10.1016/j.physleta.2025.130996.

[28] I. Vurgaftman, J. R. Meyer, L. R. Ram-Mohan, J. Appl. Phys. **89**, 5815 (2001); https://doi.org/10.1063/1.1368156.

ВПЛИВ ГЕОМЕТРІЇ КВАНТОВОЇ ТОЧКИ НА ЕНЕРГЕТИЧНІ СПЕКТРИ ДІРОК У МЕЖАХ МОДЕЛІ ЛАТТІНЖЕРА

Р. Я. Лешко[1], І. В. Білинський[1,2], О. В. Лешко[1], Т. Р. Монастирський[1], М. А. Слюсаленко[2]
[1] *Кафедра фізики та інформаційних систем,*
Дрогобицький державний педагогічний університет імені Івана Франка,
вул. Стрийська, 3, Дрогобич, 82100, Україна
[2] *Кафедра фізики, Криворізький державний педагогічний університет,*
вул. Університетська, 54, Кривий Ріг, 50086, Україна

Подано теоретичне дослідження енергетичних спектрів дірок та просторового розподілу хвильових функцій у сферичних, кубічних і конічних квантових точках GaAs/AlAs. Розрахунки виконані в межах чотиризонної моделі Латтінжера-Кона з використанням методу розкладу за тривимірними плоскими хвилями, що дає змогу точно аналітично обчислити матричні елементи гамільтоніана через перетворення Фур'є- функцій форми наноструктури. Продемонстровано, що зниження симетрії просторового обмеження від сферичної до кубічної та конічної геометрій змінює структуру енергетичних рівнів, знімаючи характерні чотирикратні та шестикратні виродження з утворенням мультиплетів нижчої симетрії. Поперечні перерізи розподілу густини ймовірності показують, що діркові стани демонструють виражені S- та P-подібні залежності завдяки змішуванню компонент важких і легких дірок. Крім того, порівняльний аналіз за сталого внутрішнього об'єму показує синій (короткохвильовий) зсув енергії основного стану. Це підтверджує, що геометричні форми з різкими межами мінімізують ефективний об'єм носіїв і посилюють квантове обмеження.

Ключові слова: діркові стани; квантове обмеження; квантові точки; метод плоских хвиль; модель Латтінжера; порушення симетрії.